

Article

Axial Compressor Mean-Line Analysis: Choking Modelling and Fully-Coupled Integration in Engine Performance Simulations

Ioannis Kolias , Alexios Alexiou , Nikolaos Aretakis  and Konstantinos Mathioudakis * 

Laboratory of Thermal Turbomachines, School of Mechanical Engineering, National Technical University of Athens, 15780 Athens, Greece; jkolias@ltt.ntua.gr (I.K.); alexioua@mail.ntua.gr (A.A.); naret@mail.ntua.gr (N.A.)

* Correspondence: kmathiou@mail.ntua.gr

Abstract: A mean-line compressor performance calculation method is presented that covers the entire operating range, including the choked region of the map. It can be directly integrated into overall engine performance models, as it is developed in the same simulation environment. The code materializing the model can inherit the same interfaces, fluid models, and solvers, as the engine cycle model, allowing consistent, transparent, and robust simulations. In order to deal with convergence problems when the compressor operates close to or within the choked operation region, an approach to model choking conditions at blade row and overall compressor level is proposed. The choked portion of the compressor characteristics map is thus numerically established, allowing full knowledge and handling of inter-stage flow conditions. Such choking modelling capabilities are illustrated, for the first time in the open literature, for the case of multi-stage compressors. Integration capabilities of the 1D code within an overall engine model are demonstrated through steady state and transient simulations of a contemporary turbofan layout. Advantages offered by this approach are discussed, while comparison of using alternative approaches for representing compressor performance in overall engine models is discussed.



Citation: Kolias, I.; Alexiou, A.; Aretakis, N.; Mathioudakis, K. Axial Compressor Mean-Line Analysis: Choking Modelling and Fully-Coupled Integration in Engine Performance Simulations. *Int. J. Turbomach. Propuls. Power* **2021**, *6*, 4. <https://doi.org/10.3390/ijtp6010004>

Received: 28 December 2020
Accepted: 23 February 2021
Published: 26 February 2021

Publisher's Note: MDPI stays neutral with regard to jurisdictional claims in published maps and institutional affiliations.



Copyright: © 2021 by the authors. Licensee MDPI, Basel, Switzerland. This article is an open access article distributed under the terms and conditions of the Creative Commons Attribution (CC BY-NC-ND) license (<https://creativecommons.org/licenses/by-nc-nd/4.0/>).

Keywords: axial compressor; mean-line analysis; choke modelling; 0D/1D coupling

1. Introduction

Development of gas turbine engines is a highly iterative procedure that involves different disciplines [1]. The first step in the development of a new engine is the preliminary design phase, where different concepts and configurations are assessed at design and off-design, steady-state and transient conditions, for identifying the optimum one that fulfills the respective performance and installation requirements. The choice is guided by seeking optimality, while not violating a number of performance, aerodynamic, structural, and installation constraints. Of all engine components, the compressor is probably the most important and critical one due to the flow physics involved. A good compressor design is essential for achieving the desired performance and operating range. Performance at a wide range of operating conditions has thus to be accurately evaluated and accounted for, as early as possible during the design of a new engine.

During the early design stages, the need for fast and reliable multi-fidelity and multi-disciplinary platforms (e.g., [2,3]), has made compressor mean-line (1D) models a valuable tool for the designer. They allow studying the effects of heat transfer [4], water evaporation, novel combustion concepts [5], and low-power operation on compressor aerodynamics [6]. In contrast to higher fidelity tools [such as 2D or fully 3D Computational Fluid Dynamics (CFD) codes], 1D tools are fast, have acceptable accuracy if appropriately tuned [5], need only a few geometry inputs, and don't need an expert user to set-up the model and calculation case. They allow designers to easily capture compressor performance trends and evaluate the effect of compressor aerodynamics on overall engine performance. For this reason, although they first appeared a long time ago, they remain of current interest and are the subject of research efforts today (e.g., [5–7]).

Mean-line codes use physically consistent modelling to capture compressor flow physics and predict performance at different conditions, using correlations and high-level indices of blade row performance. The nature of the equations they use leads to convergence problems, when the compressor works at or beyond choking conditions. Even modern 1D codes employing the approach introduced long ago, for instance in [8], still use a “pre-processing” step for determining the useful operating range “manually”. The inlet mass flow rate changes incrementally until the code producing a compressor map fails to converge as the inlet mass flow approaches or reaches the choking value. One such example is a NASA code named “OTAC” (Object-oriented Turbomachinery Analysis Code) [9,10], that conducts mean-line or stream-line design and off-design performance calculations, for radial- or axial-flow turbomachines. For a speed-line, the flow where one (or more) compressor blade rows choke is taken equal to the value for which the code fails to converge [10]. In another code for compressor mean-line calculations, also developed at NASA [11], the working mass flow range is determined iteratively by varying the incidence angle of the first rotor row and for any given speed the maximum flow is identified when the code fails to converge.

Attempts to modify the set of mean-line equations so that turbomachinery performance models can work without convergence problems within the choked portion of the map have been demonstrated successfully only on multi-stage turbines [12]. Because of the more complicated nature of the flow involved, the real challenge in modelling compressor choke “lies primarily in understanding the mechanisms causing it”, as stated by Hendricks in [12]. In that direction, various efforts were made to model compressor choking. Arolla et al. [13] described a low-order approach for modelling the blade row throat passage choke for subsonic and supersonic inlet conditions. They also proposed a method for producing the vertical portion on the characteristics map, by introducing additional losses at the last choked blade row until the compressor back pressure was attained or a downstream blade row choked. They demonstrated successfully the application of their method on a single-stage fan. Cadrecha et al. [14], used simple flow equations to first identify the conditions (in terms of flow Mach number) that lead blade rows and ducts to choke. They then formulated a bisection method for solving the system of mean-line equations at subsonic, supersonic, and choke conditions. They also described a modelling approach for extending the choked portion of the map characteristics where they increased the losses of the duct following a choked blade row, until the last row or the compressor exit chokes. The proposed methods were exemplified on a “dummy” geometrical model of a multi-stage turbine with zero losses and demonstrated for the case of a single-stage compressor for which a performance map was produced for three rotational speeds.

In the present paper, a Mean-Line Code (MLC) is developed that combines and extends the modelling approaches of [13,14] for choke modelling. Choke is examined by considering both throat and flow annulus (in [13,14] the one or the other alone is considered). Appropriate indices are introduced to quantify how far any blade row or annulus operates from choke. The maximum flow the compressor can deliver is established by zeroing these indices using a robust numerical procedure. Overall, a physically consistent, transparent, and fully automated procedure is proposed, for producing the entire compressor performance map. For the first time in the open literature, multi-stage compressor maps are generated with inter-stage flow features captured in the full operating range, including the “vertical” part of the characteristics.

The developed MLC can be integrated in an overall gas turbine engine model, replacing the traditional performance maps. Such a replacement offers possibilities for more accurately representing overall engine performance, while it provides additional flexibilities for handling effects that are very cumbersome to introduce when legacy maps are employed. Example effects of this type are map variability versus inlet temperature, variable geometry, variable inter-stage bleeds, water ingestion or inter-stage injection, incorporation of heat transfer effects at stage level.

Although mean line codes have been presented in the public literature, there are no cases where such a code is developed, integrated, and used for simulation in a 0D cycle analysis in a consistent, transparent and robust way similar to that of conventional 0D components. Typically, 0D and 1D codes are developed independently of each other (sometimes using different programming languages, gas calorific properties, solvers, etc.), which results in thermodynamic and numerical inconsistencies between them. NASA's code OTAC [9,10] is an exception to this, but up to now there has been no publication demonstrating its coupling with an engine model. Generally, there are three approaches for coupling the 1D (or higher fidelity) and 0D cycle analysis codes [15,16]:

- De-coupled: the higher fidelity code is used to generate compressor characteristics which are then used as data in the conventional 0D cycle code (e.g., [3]).
- Semi-coupled: An iterative scheme is implemented, where the 0D cycle analysis provides boundary conditions to the 1D code and then the 0D component performance is updated according to the higher fidelity results. This loop is repeated until 0D and 1D performance is matched within a user-defined tolerance (e.g., [17]).
- Fully-coupled: The higher fidelity component is fully integrated in the cycle analysis (e.g., as an external object) directly replacing the corresponding 0D component [18].

In the de-coupled approach, the mathematical formulation of the 0D cycle analysis is not affected, but the map is valid for the geometry and secondary effects (bleed-off takes, inlet temperature, heat transfer, water injection/ingestion) for which the map is generated, while map interpolation reduces accuracy. Semi- or fully-coupled approaches necessitate a change in the mathematical formulation of the conventional cycle model and/or the model building logic, which can affect simulation robustness. The exchange of information between the codes impacts speed of execution. In the fully-coupled approach, map interpolation is not needed, avoiding thus accuracy compromise.

A versatile fully-coupled approach for integrating a mean-line code in an engine model is proposed in the present paper. A 1D code is developed as a stand-alone component in the same environment as 0D components and uses the same interface and functions for numerical, working fluid model and thermodynamic calculations. This ensures modelling homogeneity and mathematical robustness during mixed-fidelity calculations while facilitating code extendibility and maintainability. The component can operate either as 0D or 1D, preserving the mathematical formulation of existing 0D performance calculations and handling choking at component and engine level, and accounts for changes in geometry and bleed off-takes. Gas modelling with either variable or constant gas properties can be selected, if execution speed up is needed, e.g., during optimization and design space exploration studies.

The implementation is exemplified through steady state and transient simulations of a turbofan model at both altitude and sea-level conditions where the component is used as the high-pressure compressor (HPC), for both 0D and 1D modes.

In the following, the 1D modelling and the methodology for modeling compressor choking and generating the map are first presented, followed by the description of how the component produced is integrated in an engine level.

2. Mean-Line Code (MLC)

The Mean-Line Code for performance analysis of axial-flow, multi-row compressors, was developed and validated in the same environment as the conventional 0D components for turbomachinery performance simulations, used to build overall engine models. The environment used was the Propulsion Object Oriented Simulation Software (PROOSIS) with its TURBO library [19,20]. Existing 0D compressor components were extended to add the 1D capability. The new component developed inherits the same fluid and mechanical interfaces to enable interconnections with other components and/or systems, and the same functions for numerical, fluid flow, and thermodynamic properties calculations. A transparent integration in engine cycle analysis calculations, without affecting the mathematical

formulation and the simulation robustness, is thus ensured. A brief description of the 1D modelling is given below.

For known compressor geometry [i.e., flow annulus hub and tip radii, basic dimensions of blades and blade metal angles at leading (LE) and trailing edges (TE)], inlet flow conditions (\dot{m}_{in} , $T_{t,in}$, $p_{t,in}$), and compressor speed (N), the MLC calculates the compressor exit total pressure and temperature by conducting a row-by-row calculation, applying loss and deviation models for individual blade rows. The building blocks of MLC are the Blade Row Module (BRM) modelling individual blade rows, and the Inter-Volume Module (IVM), modelling the duct after a blade row.

In the IVM, gas bleeds are applied through mass and gas composition continuity, annulus radius changes are taken into account through a moment of momentum balance, while heat transfer, water-vapor injection (i.e., gas mixing), and pressure loss effects have also been foreseen. BRM models any type of blade row [rotor, stator, inlet guide vanes (IGVs), of variable or fixed geometry] and establishes the row outlet conditions by solving iteratively the set of equations formed by mass and gas composition continuity, the conservation of energy, and loss and deviation correlations introduced to calculate the flow across the row. More specifically, the aerodynamic performance of diffusing rows is modelled in terms of Lieblein's diffusion and equivalent diffusion factors [21], where the design incidence and deviation angles are calculated using Herrig's and Lieblein's correlations [21], respectively. The blade row deviation angle (δ) and, thus, outlet flow angle, is estimated using Swan's model [22]. Across a row, the Euler pump equation for rotors or the conservation of total enthalpy for stators gives the outlet total enthalpy, while the exit total pressure is estimated using a total pressure loss coefficient (ω). In ω , profile, secondary, and endwall losses are accounted for according to Aungier [21], clearance losses are modelled using the simplified model of Lakshminarayana [23], shock losses are calculated according to Steinke's shock model [24], while Mach and Reynolds number effects are taken into account following Aungier [21] and Koch et al. [25], respectively. For IGVs, δ and ω are calculated according to Banjac et al. [26]. The loss and deviation models used in MLC are fully tunable through appropriate scalars, the value of which can either be the default one, a user input, or evaluated numerically. The code is also fully scalable, in the sense that the user can switch on or off any of the above loss sources, and can easily introduce customized loss and deviation models. A summary of the default loss and deviation correlations mentioned above can be found in Appendix A.

Finally, the code has the possibility to perform calculations with variable or constant gas properties for each blade row. In the latter case, specific heats ratio (γ) and specific heat capacity (c_p) for a blade row, are calculated based on appropriate local temperatures. It was found that the results of such calculations are very close to those of using the full gas model when the blade row inlet temperature for stators, and average inlet-outlet temperatures for rotors ($(T_{t1} + T_{t2})/2$), is employed. The local temperature at any station along the compressor is evaluated by assuming that each stage, i , achieves the same temperature rise $\Delta T_{t,i}$, which is given by the following formula:

$$\Delta T_{t,i} = \frac{\left(\overline{PR}^{(\gamma-1)/(\eta_p \gamma)} - 1\right) T_{t,in}}{Z_{stg}} \quad (1)$$

assuming a polytropic efficiency of $\eta_p = 90\%$, $\gamma = 1.4$, and the compressor design pressure ratio value as the average total pressure ratio \overline{PR} . Only the thermodynamic properties are calculated using the local γ and c_p , instead of using the full expressions of fluid and thermodynamic models that calculate gas properties as function of temperature and gas composition. The magnitude of differences of the results using the two approaches will be presented in the results section.

3. Choke Modelling

A 1D compressor model for off-design performance analysis must be able to determine not only the maximum flow a compressor can deliver, but also the performances over the choked region of operation. Convergence problems in obtaining the solution of the mean-line equations near or beyond choked conditions, must be resolved [12,14].

In the present paper, choke conditions are modelled by introducing indices that quantify the “distance” of an operating point along a speed-line from the corresponding limiting value. For this reason, four dedicated indices are defined, three at blade row level and one at compressor level. An appropriate functional of these indices is defined, which is numerically zeroed for estimating the choked mass flow. Once the maximum mass flow for a speed-line is obtained, the choked part of the map characteristics is established. The procedure followed is presented below.

3.1. Indices for Annulus and Throat Passage Choke Modelling

For modelling annulus choke, three indices are defined, two at each blade row and one at compressor exit:

$$index_{br,inan} = (\dot{m}_1^* - \dot{m}_1) / \dot{m}_1^* \quad (2)$$

$$index_{br,outan} = (\dot{m}_2^* - \dot{m}_2) / \dot{m}_2^* \quad (3)$$

$$index_{ex} = (\dot{m}_{ex}^* - \dot{m}_{ex}) / \dot{m}_{ex}^* \quad (4)$$

Indices “*br, inan*” and “*br, outan*” express, respectively, how far is the actual mass flow that passes through the blade row inlet and outlet annuli from the choked one, while index “*ex*” expresses the same condition for the compressor exit. In each equation, the choked mass flow is calculated from local critical properties:

$$\dot{m}^* = \rho^* W^* A \cos \beta \quad (5)$$

where A is the flow annulus cross-sectional area, and the critical static density and sonic velocity are calculated for the local total pressure and temperature conditions.

Modelling of the blade row throat passage choke was achieved by introducing one more index:

$$index_{br,th} = (\beta_1 - \beta_1^*) / \beta_1^* \quad (6)$$

This quantity indicates how far the actual flow angle β_1 is from a minimum value, β_1^* , below which the blade row throat passage chokes. For calculating the critical blade row inlet flow angle, β_1^* , two flow conditions were considered at the blade row inlet: subsonic and supersonic. For modelling them, the approach of Cumpsty and Freeman [27,28] was followed, as presented in Appendix B.

A schematic diagram of the flow stations where the choke indices are defined and estimated is shown in Figure 1 below. For any set of compressor inlet conditions (\dot{m}_{in} , $T_{t,in}$, $p_{t,in}$) and N , MLC also estimates $index_{br,inan}$, $index_{br,outan}$, and $index_{br,th}$ for every blade row, and $index_{ex}$ for the compressor exit. For a compressor to operate away from choke all indices, Equations (2)–(4) and Equation (6), should be positive.

3.2. Estimating Choke Point

A secant method is used to establish numerically the compressor choking mass flow rate, since it was found to be the most robust. For any compressor speed N and inlet conditions $T_{t,in}$, $p_{t,in}$, the secant method updates the compressor inflow, \dot{m}_{in} , until the functional G of Equation (7) is zeroed or two successive estimates for \dot{m}_{in} differ less than a specified tolerance,

$$G = index_{min} - \varepsilon \quad (7)$$

where $\varepsilon > 0$ a number with small value set by the user and $index_{min}$ is the global minimum index:

$$index_{min} = \min [(\text{index}_{br,min})_{\forall br'} | \text{index}_{ex}] \quad (8)$$

where the minimum index for the blade row, $index_{br,min}$, is:

$$index_{br,min} = \min (|index_{br,inan}|, |index_{br,outan}|, |index_{br,th}|) \quad (9)$$

To avoid numerical solutions in the windmilling region of compressor operation, a constraint is also imposed to the overall total pressure ratio, which should be greater than a minimum, user-specified value $PR_{min} > 1$.

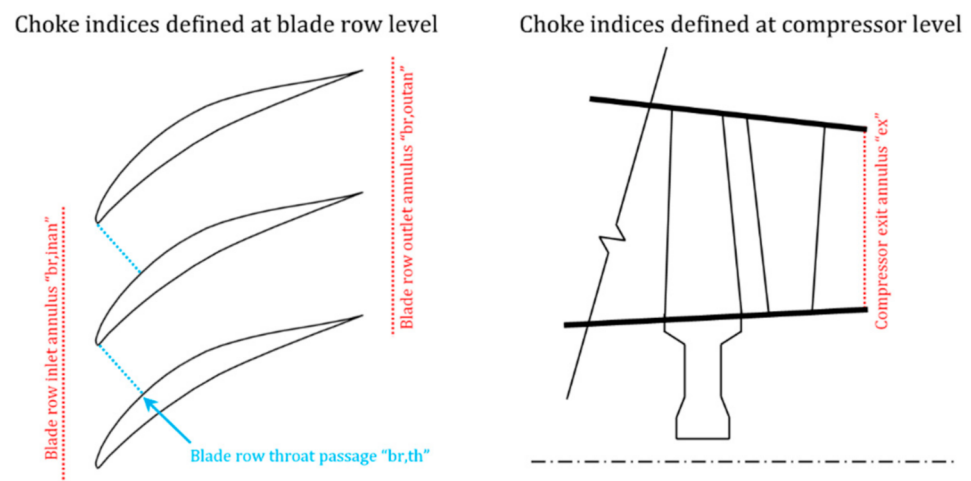


Figure 1. Schematic representation of the flow stations where the choke indices are defined.

3.3. Choked Part of a Speed-Line

The choked part of a speed-line is vertical to the mass flow axis, since it is characterized by a constant corrected mass flow rate. A mean-line calculation should provide the flow characteristics, pressure, temperature, velocity magnitude and direction, at the inlet and outlet of each blade row, along a multistage compressor flow path for operation in this part. The approach we follow for determining these quantities, when the compressor pressure ratio becomes lower than its value at the onset of choke, was based on the assumption that the flow pattern in the part of the compressor downstream of the choked row will be formed so that pressure losses are such that the outlet pressure matches a back pressure specified. Thus, the flow before the choked row is considered frozen, pressure losses are incrementally added to the choked blade row, and the flow along the downstream blade rows is computed until the compressor back pressure is attained or a downstream row becomes choked. If the compressor back pressure is not reached, but a downstream row chokes, then the same procedure is repeated for the new choked row. This approach is similar to the one used by Arolla et al. [13], who applied it to the case of a single-stage fan, but gave no insight as to how the flow conditions will evolve when choke occurs along a multi-stage compressor.

For a compressor map to be generated, the last point on the vertical portion of the map characteristics that corresponds to the minimum pressure ratio the compressor can attain operating at the maximum \dot{m}_{in} , is established first. Starting from the first choked blade row, an iterative scheme is employed that modifies the losses of the choked row until a downstream row chokes. The same procedure is then repeated successively for every downstream row that chokes until, eventually, the compressor exit becomes choked. In any case, the last pressure ratio is taken equal to the maximum value between the PR established in the above iterative procedure, and a user-defined value $PR_{min} > 1$ for avoiding solutions in the windmilling regime. Finally, the vertical portion of the map

characteristic is refined for any user-defined number of pressure ratio values between the first and the last one, following the algorithmic logic shown in Figure 2.

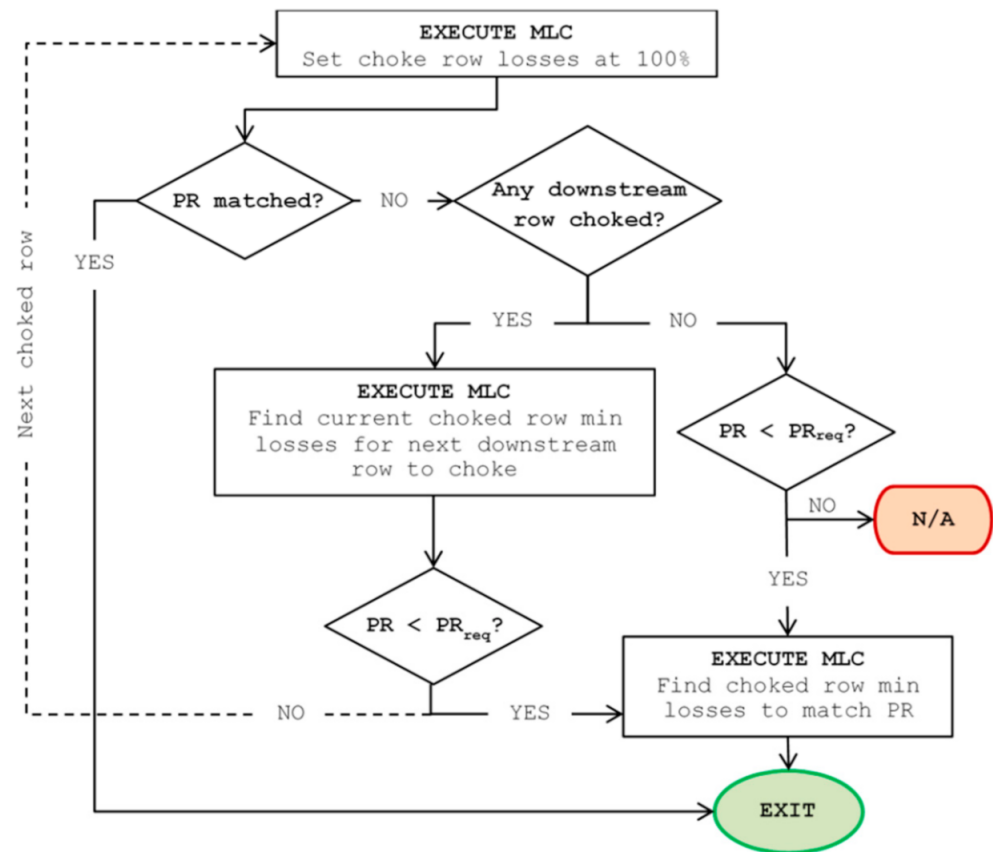


Figure 2. Mean-Line Code (MLC) flow-chart to establish the 1D performance in the choked region.

4. 1D Component Model for Integration in 0D Cycle Analysis

In its simplest form, a conventional 0D compressor component (Figure 3a) establishes performance by reading a set of tables (a map) that return corrected mass flow rate (\dot{m}_c), isentropic efficiency (η) and pressure ratio (PR) for given values of the auxiliary map parameter (BETA) [29] and corrected speed relative to design ($NcRdes$). BETA is an independent (or algebraic) variable at engine model level that the numerical solver (e.g., Newton-Raphson) adjusts in order to ensure consistent operation of engine components [30].

MLC, on the other hand, requires mass flow rate \dot{m} and compressor speed N as inputs and returns η and PR . For this reason, the new component implements a two-step, hybrid approach, enabling it to be used in either 1D or 0D mode (user-defined option), while also maintaining the traditional 0D algorithmic logic when the 1D mode is employed. This requires the use of a map that is generated with the MLC through a dedicated simulation case using the modelling approach described above. This is a necessary pre-processing step before the component can be used. Actually, a multitude of maps are generated for a range of compressor inlet temperatures $T_{t,in}$ [including of course the International Standard Atmosphere (ISA) conditions] in an effort to improve calculation accuracy (irrespective of operating mode) since conventional gamma corrections [note that, typically a map is generated for a given compressor inlet temperature (e.g., at ISA conditions) and gamma corrections are applied to account for the effects of different temperatures during simulation] are not sufficient [31]. Then, when the component works in 1D mode, BETA is still used as an algebraic variable for reading the map of the pre-processing step to obtain a mass flow rate value \dot{m} . Next, this \dot{m} value is used to execute the MLC and derive the compressor performance (Figure 3b). The MLC-generated map

provides the required \dot{m}_c -BETA relationship, which otherwise would have to be established through multiple MLC executions during every cycle calculation. Furthermore, the map acts as a reference in order to correctly account for the current operating conditions, as will be explained in the following.

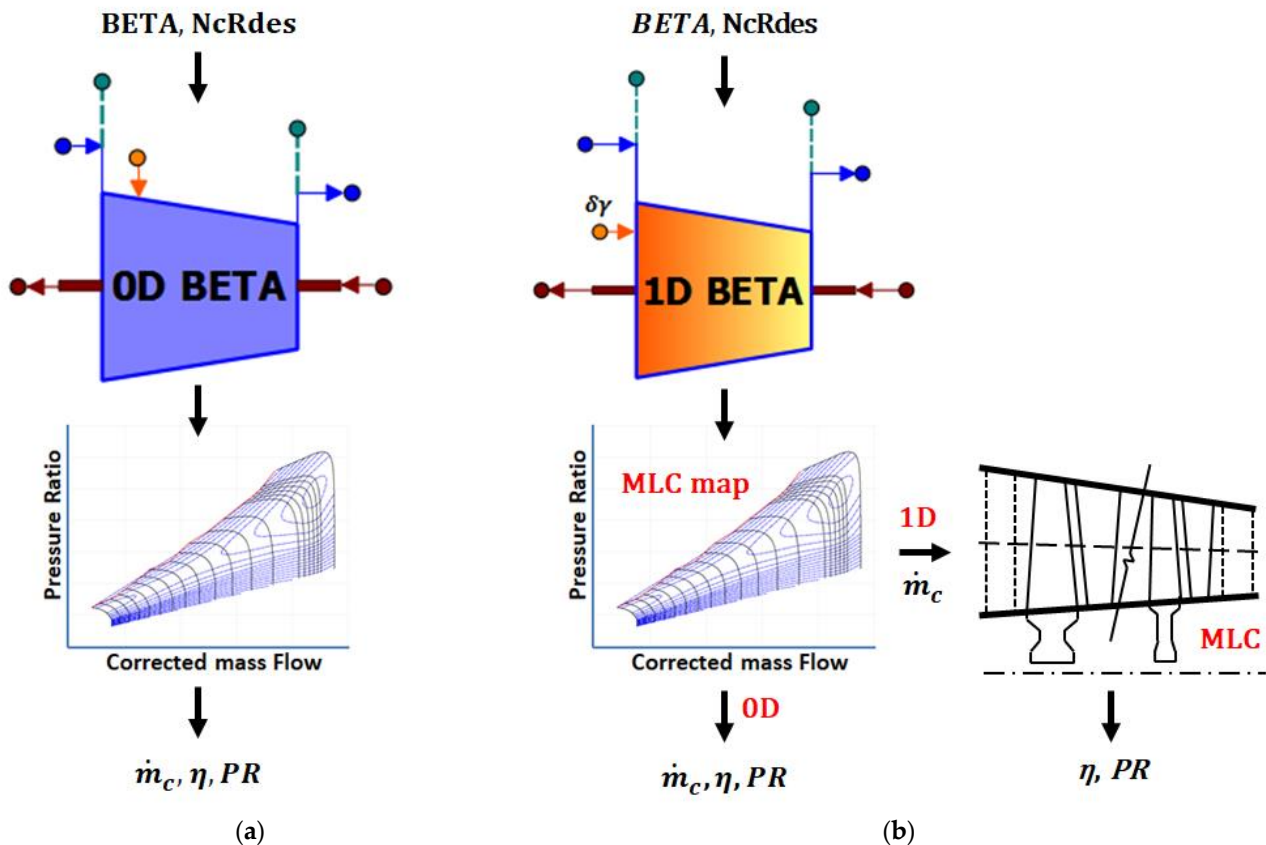


Figure 3. Compressor performance using (a) conventional 0D and (b) new 0D/1D component.

During the pre-processing step, a table is also derived with the values of BETA ($BETA_{choke}$) below which choking occurs. The independent variables for reading this table are compressor corrected speed $NcRdes$ and $T_{i,in}$. So, when the component operates in the 1D mode, the current value of BETA is compared with $BETA_{choke}$ to determine if operation is in the choked region or not.

If unchoked, the value of mass flow rate is obtained from the map (\dot{m}_{map}) for the current BETA, $NcRdes$, and $T_{i,in}$. To account for changes between 1D performance for the current compressor operating conditions and map (generated for some reference conditions), the 1D code is executed once to find the first point in the choke line (\dot{m}_{MLC}^*) for the current conditions (see Figure 4). A correction is then performed in the value of mass flow \dot{m} for which the 1D code is executed in the unchoked part to account for any shift ($\dot{m}_{MLC}^* - \dot{m}_{map}^*$) in the position of the choke line (compared to map value \dot{m}_{map}).

On the other hand, if $BETA < BETA_{choke}$, the logic presented in Figure 2 is implemented, where for $\dot{m} = \dot{m}_{MLC}^*$, the required PR is the one obtained from the map, but corrected for the current compressor operating conditions, as illustrated in Figure 4. The algorithm establishes the choked row losses that will result to the required compressor exit pressure. The complete algorithmic logic of the new 0D/1D component is depicted in the flowchart of Figure 5.

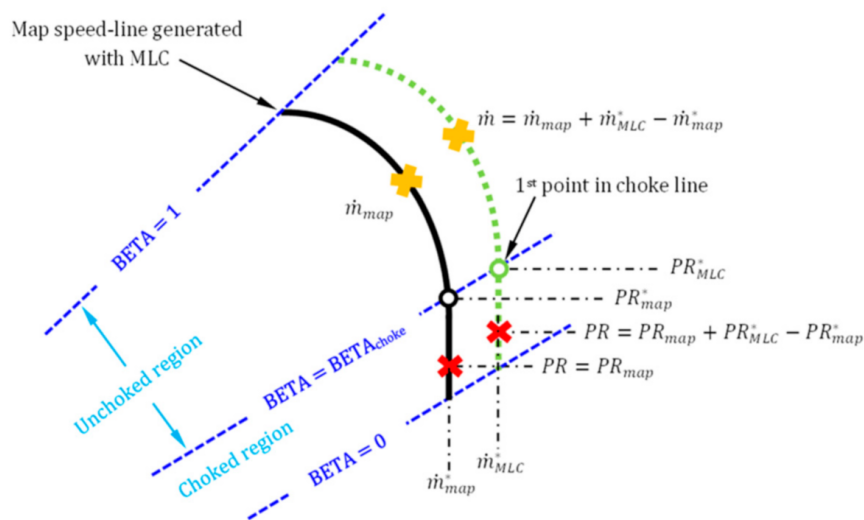


Figure 4. Accounting for current operating conditions.

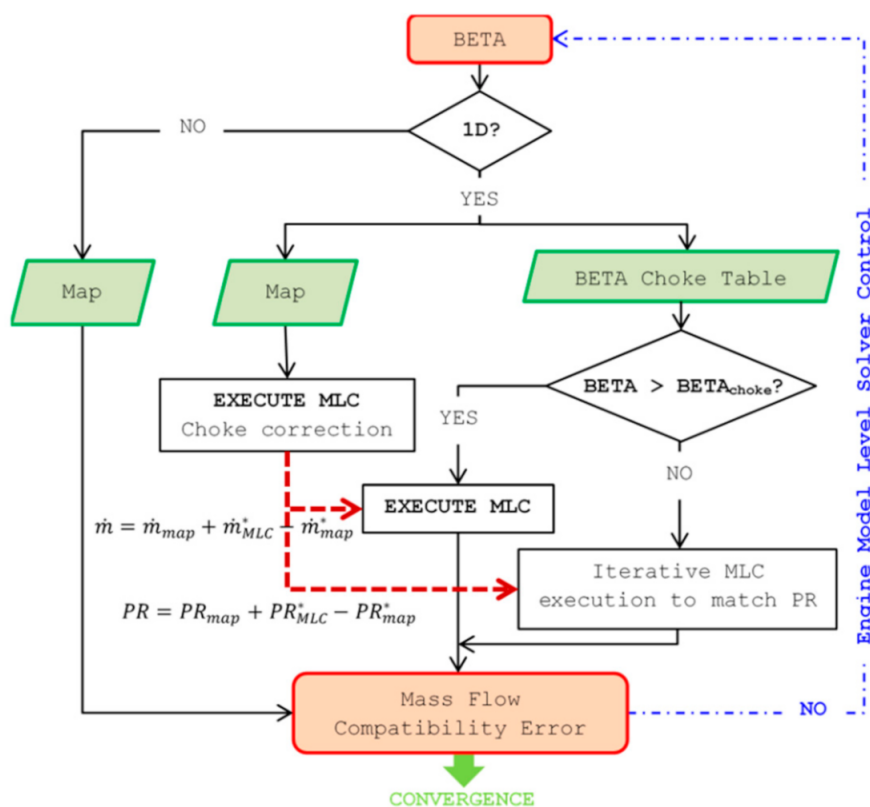


Figure 5. Algorithm flow chart to establish the auxiliary map parameter (BETA) for mass flow compatibility.

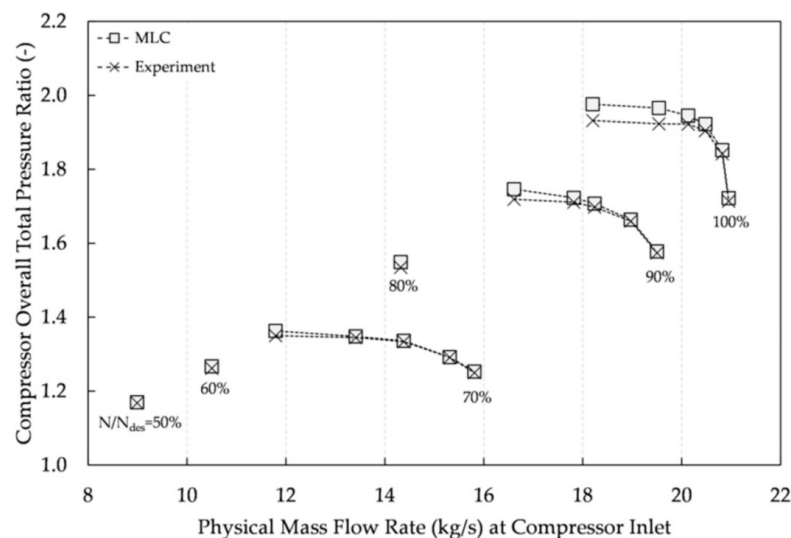
5. Example Compressor Map Results

The MLC choke modelling and the 1D model integration capabilities are exemplified using the geometries of two multi-stage compressors, NASA’s ISG-74A [32] and NASA/GE’s E³ HPC [33]. NASA’s ISG-74A is a 3-stage transonic, high-speed compressor developed and tested during the 80s, while NASA/GE’s E³ HPC is a 10-stage transonic, high-speed, high-aerodynamic loading compressor developed and tested during the late 70s-early 80s. Basic geometry and performance details for both compressors are summarized in Table 1.

Table 1. Basic geometry and performance information for the example multi-stage compressors.

	NASA ISG-74A [32]	NASA/GE E ³ HPC [33]
Design Pressure Ratio	4.474	25
Design Inlet Mass Flow (kg/s)	29.71	54.40
Design Rotating Speed (rpm)	16042.3	12416.5
No. of Stages	3	10
No. of Rotor Rows	3	10
No. of Stator Rows	4 [including inlet guide vanes (IGVs)]	11 (including IGVs)

Note that the default loss and deviation models used in MLC were mostly developed on the basis of cascade tests in subsonic wind-tunnels during the early 50s and, hence, they cannot capture the performance of current transonic compressors, as explained in [5]. MLC offers the capability of calibrating numerically these models for representing current compressor aerodynamics. An example of reproducing a compressor map through such a calibration is given in Figure 6 for NASA's "Stage-35" [34]. Thus, it is shown that the method proposed contains the flexibility to adapt to and correctly model the performance of axial compressors. We will not further discuss this aspect of the method, since the focus of the present work is to discuss the features of the process for establishing choked operation and its integration in engine models. Therefore, the geometries of the compressor test cases used serve merely as a demonstration of the capabilities developed and not for validating MLC against publicly available data. In what follows, MLC is executed with its default loss and deviation models.

**Figure 6.** Comparison between MLC prediction and experimental map for NASA's "Stage-35" [34] compressor.

5.1. Choke Modelling

Choke modelling capability is demonstrated on the geometry of a 3-stage transonic compressor [32], see Table 1. For easy reference in the discussion, the following designation is used for the compressor blade rows: IGV-R1-S1-R2-S2-R3-S3, where "R" stands for rotors and "S" is for stators.

The map produced by the MLC is shown in Figure 7. It was produced for standard-day conditions, assuming axial flow at the compressor inlet, zero bleed extractions, at the design IGVs-stators setting. The choked mass flow rate was calculated using a value of $\varepsilon = 0.001$ in Equation (7), while a lower bound on the total pressure ratio of $PR_{min} = 1.001$ was imposed when establishing both the first and the last point on the choked portion of the map characteristics. Between stall and choke, PR was calculated for 11 equally distributed values of \dot{m}_{in} along each speed-line.

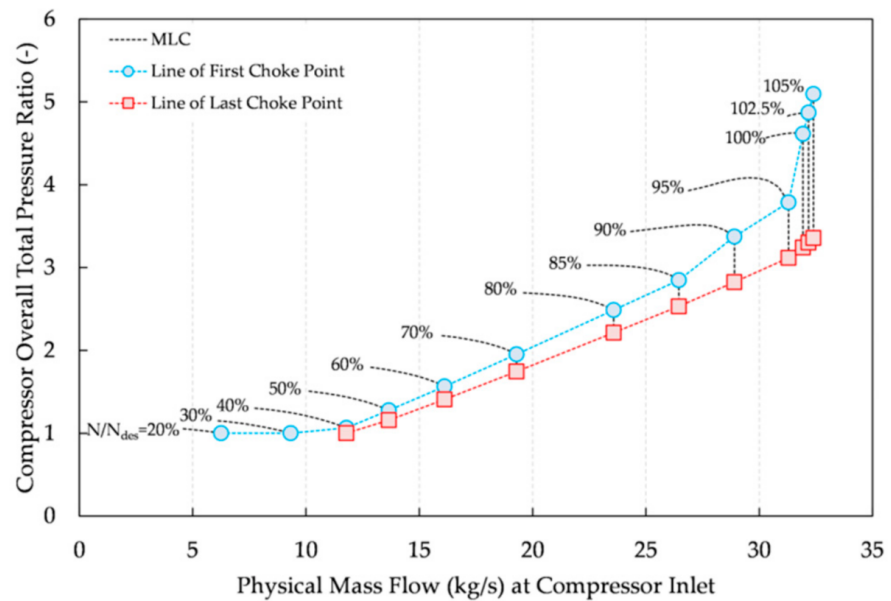


Figure 7. MLC pressure ratio map for the example 3-stage compressor geometry [32].

The lines that connect the respective first and last choke points on every speed-line are also presented in Figure 7, defining the domain where the compressor operates at the maximum inlet mass flow. For $N/N_{des} = 20\%$ and 30% the maximum flow is established from the limiting pressure ratio value of $PR_{min} = 1.001$ and, therefore, no vertical portion of the characteristics exists. The compressor works unchoked at these two speeds. Numerically, this means that the secant method cannot zero the functional expressed in Equation (7) for the value of $\epsilon = 0.001$ while satisfying the constraint $PR > 1.001$. At both these points, $index_{R3,outan}$ has the minimum value which is about two orders of magnitude greater than the value of $\epsilon = 0.001$ for which choking is assumed to numerically occur. For $N/N_{des} = 40\%$, there is a narrow region on the map characteristic where the compressor can work at the maximum mass flow. Here, the compressor chokes for the first time at the throat of S3, while the last choke point is established from the constraint $PR_{min} = 1.001$ which is met before the compressor exit annulus becomes choked. Table 2 summarizes the rows and stations where the first and last choke points occur for the speed-lines with $N/N_{des} > 40\%$.

Table 2. MLC first and last choke point results for the example 3-stage compressor geometry [32].

N/N_{des}	First Choke Point Row-Station	Last Choke Point Row-Station
50–85%	S3-Throat	Compressor exit
90–95%	R3-Throat	Compressor exit
100–105%	R1-Throat	Compressor exit

To illustrate in more detail how the first choke point is established numerically, the 85% speed-line is used as an example. In Figure 8, the choke indices values are plotted against \dot{m}_{in} as it increases towards the choking value. Figure 8a shows the variation of the global minimum index ($index_{min}$) and the variation of the minimum blade row index ($index_{br,min}$) for all blade rows, while Figure 8b shows the variation of the individual S3 indices, $index_{S3,inan}$, $index_{S3,outan}$, $index_{S3,th}$, and $index_{S3,min}$.

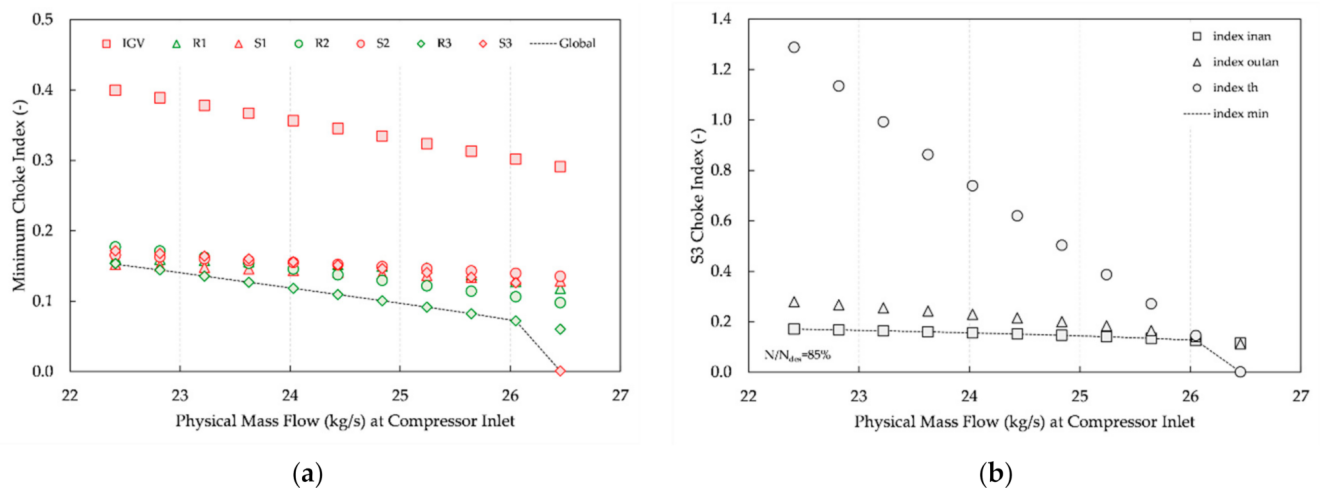


Figure 8. Choke indices variation for the example 3-stage compressor geometry [32], for $N/N_{des} = 85\%$: (a) Minimum choke indices variation and (b) S3 individual choke indices variation against compressor inlet mass flow.

From Figure 8a, it is seen that $index_{min} = index_{R3,min}$ for \dot{m}_{in} between 22 and 26 kg/s, while in the same mass flow range the distance between $index_{R3,min}$ and the values of all other indices either increases or remains constant as \dot{m}_{in} increases. This means that, if the compressor were to choke for a \dot{m}_{in} value between 22 and 26 kg/s, it would be due to R3 becoming choked. As, however, \dot{m}_{in} approaches the choking value (≈ 26.5 kg/s), $index_{S3,min}$ experiences an abrupt value drop and becomes less than $index_{R3,min}$. This in turn results in an abrupt drop in the value of $index_{min}$, causing the compressor to eventually choke for the first time at S3 as its value becomes equal to that of $index_{S3,min}$. The reason for the drop in $index_{S3,min}$ value can be found in Figure 8b. It is observed that $index_{S3,min} = index_{S3,inan}$ for \dot{m}_{in} between 22 and 26 kg/s and, using the same rationale as before, if S3 were to choke for a \dot{m}_{in} in this range it would be due to the choking of the row inlet flow annulus. However, the distance between $index_{S3,inan}$ and the other indices decreases as the mass flow increases and, for a \dot{m}_{in} value slightly greater than 26 kg/s the difference between $index_{S3,th}$ and $index_{S3,inan}$ finally becomes negative, therefore causing the drop in $index_{S3,min}$ value and S3 to choke at the passage throat instead as \dot{m}_{in} approaches the choking value.

The absolute flow Mach number at S3 inlet is shown to be subsonic, for all $22 \leq \dot{m}_{in} \leq 26$ kg/s, in Figure 9a. As the flow Mach number increases, the minimum flow angle required for the throat to become choked (β_1^*) increases as well, while the absolute flow angle at the inlet of S3 decreases until the two become equal within the specified tolerance of $\varepsilon = 0.001$ and, therefore, the throat passage choking for S3 is realized for subsonic conditions. This is in contrast, for instance, to the R1 throat passage choking for $N/N_{des} = 100\%$ where, as seen from Figure 9b, the relative flow Mach number at R1 inlet is supersonic for $30 \leq \dot{m}_{in} \leq 32$ kg/s and the throat passage chokes for supersonic conditions with attached shocks.

The method to extend the choked part described in Section 3.3 is exemplified considering the speed-lines 100%, 102.5%, and 105%. In all three speed-lines, both the first and last choke points occurred at the throat passage of R1 and the compressor exit, respectively. Thus, these speed-lines were a good example for viewing how the choke point moves from R1 (almost at the compressor inlet) until it reaches the compressor exit flow annulus. Figure 10 shows the outcome of the procedure of the flow chart in Figure 2. It shows the “iso-choke” lines that denote the different rows and stations that choke successively as the compressor PR is reduced. It is shown that choking advances from R1 to R2 to R3 to S3 until the compressor exit is reached and the minimum pressure ratio for which the compressor can work is attained. For all blade rows, choking occurred at the respective throat passage. For all three rotors, the flow regime at the respective inlet is supersonic

with attached shocks, while the flow at S3 inlet is subsonic. An overall pressure ratio map showing the “iso-choke” lines for the case of the example 3-stage compressor geometry is presented in Figure 11.

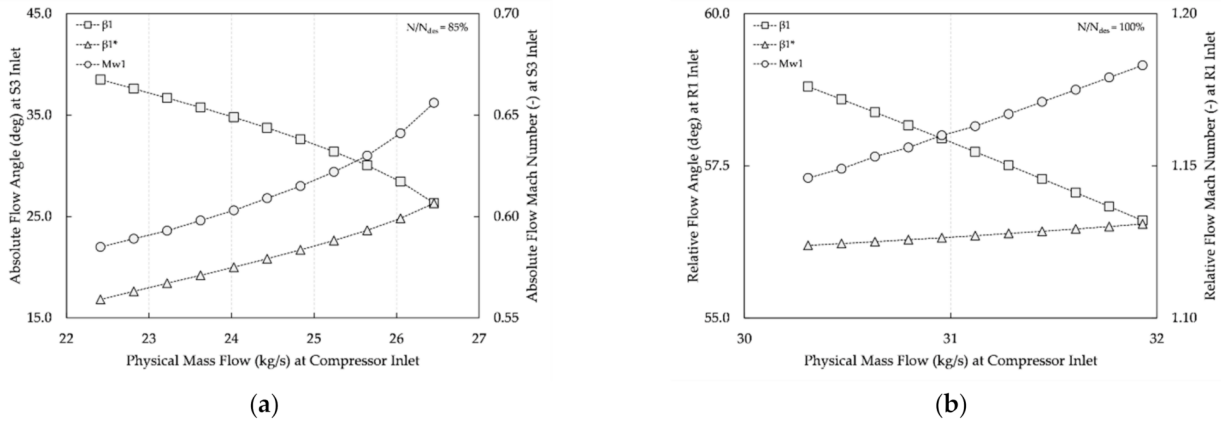


Figure 9. Throat passage choking for (a) S3 (at 85% compressor speed) and (b) R1 (at 100% compressor speed), for the example 3-stage compressor geometry [32].

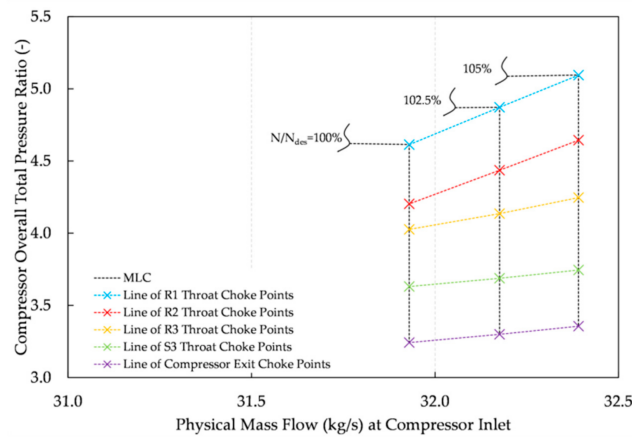


Figure 10. “Iso-choke” lines for the 100%, 102.5%, and 105% speed-lines for the example 3-stage compressor geometry [32].

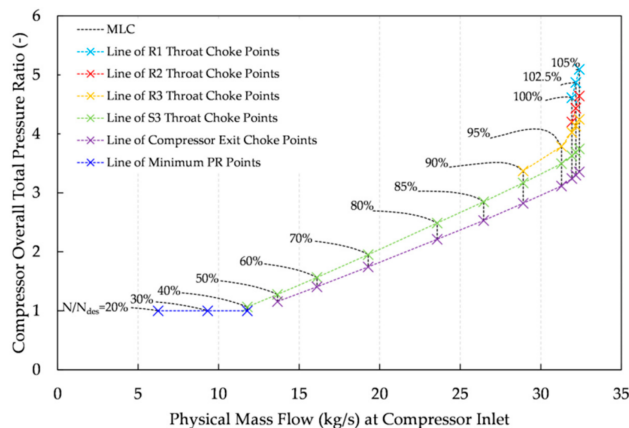


Figure 11. MLC pressure-ratio map for the example three-stage compressor geometry [32] showing the “iso-choke” lines.

5.2. Example of MLC Integration in Engine Model

For demonstrating the integration and simulation of the newly developed 0D/1D component in an engine performance model, the case of a two-spool, unmixed flow turbofan engine was considered where the component is used for the HPC. Since the fluid and mechanical interface of the component in hand is identical to the corresponding 0D one, it can be connected to other relevant 0D components without any changes in the model building procedure, as shown in the schematic diagram of Figure 12.

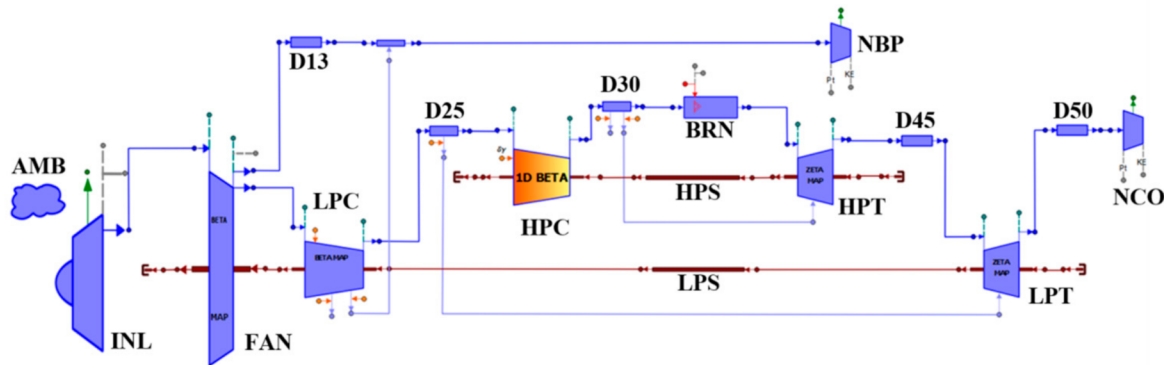


Figure 12. Schematic diagram of turbofan model with 1D compressor component. In the same diagram the components for representing the atmosphere (AMB), engine inlet (INL), fan (FAN), low- (LPC) and high-pressure compressor (HPC), low- (LPT) and high-pressure turbine (HPT), low- (LPS) and high-pressure shaft (HPS), burner (BRN), core (NCO) and bypass nozzle (NBP), and interconnecting ducts (D13/25/30/45/50), are also shown.

Similarly, the mathematical formulation of this mixed-fidelity engine model is identical to the conventional 0D performance case, in terms of boundary conditions (only one handle variable was required, e.g., thrust or fuel flow rate), algebraic (turbomachinery component map parameters, bypass ratio, inlet mass flow rate) and dynamic (low and high pressure spool rotational speeds) variables.

The 1D component was set to represent the NASA/GE E³ HPC as far as the necessary stage, blade, and geometric input data required [33]. Following the pre-processing step, a map (Figure 13) is generated for four compressor inlet temperatures, covering the expected range for the considered application ($T_{t,in} = 200, 288, 400, \text{ and } 500 \text{ K}$). In fact the map is a set of 3D tables describing \dot{m}_c , η and PR in terms of BETA, $NcRdes$, and $T_{t,in}$. In addition, the table of BETA for each corrected speed below which choking occurs is produced ($0.20 < BETA_{choke} < 0.27$).

An engine design calculation was performed first in order to calculate at cruise conditions ($ALT = 10668 \text{ m}$, $M = 0.85$) the scaling factors for the 0D map components [fan, booster, high- (HP) and low-pressure (LP) turbines] and the throat areas of the convergent bypass and core nozzles. The boundary variables in this calculation include the location of the design point on the maps of the 0D map components, their polytropic efficiencies, the pressure ratio values of the fan (bypass and core) and booster, the bypass ratio, the LP spool rotational speed, and the turbine inlet temperature. To obtain a valid operating point for the HPC, BETA and relative corrected speed were specified (in analogy to specifying the design point on the 0D map component). The values of the main engine cycle parameters are included in Table 3.

Off design simulations were then performed to generate a steady-state operating line and a transient square cycle between low and high power conditions at both altitude ($ALT = 10668 \text{ m}$) and Sea-Level Static (SLS) conditions. Simulations are performed in both 0D and 1D mode for the HPC component and in the latter case, for either variable or constant gas properties. For simulations with constant γ and c_p , an overall total pressure ratio value was assumed equal to the HPC PR of the previous calculated point.

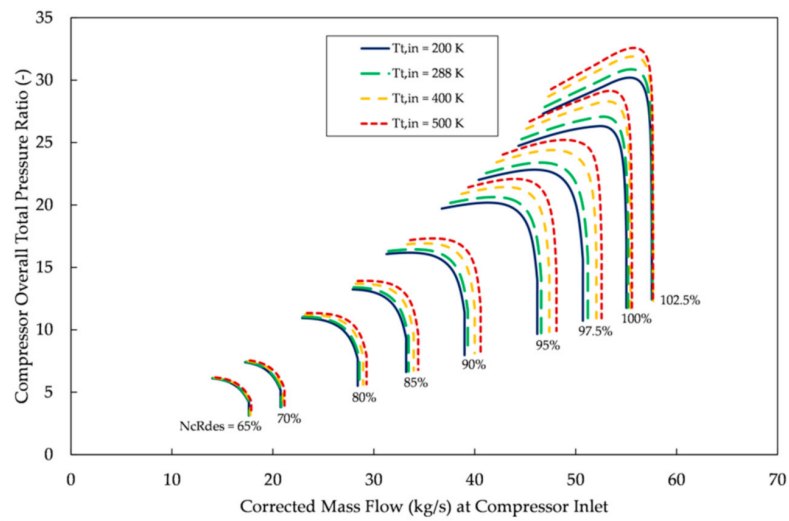


Figure 13. MLC generated map for different compressor inlet temperatures.

Table 3. Selected engine cycle parameters at design point.

Parameter	Value
Engine Net Thrust (kN)	59.2
Engine Overall Pressure Ratio (-)	56.1
Engine Bypass Ratio	8.85
Engine Specific Fuel Consumption (g/kN·s)	15.52
Engine Inlet Mass Flow Rate (kg/s)	463.5
Fuel Flow Rate (kg/s)	0.918
High-Pressure Compressor (HPC) Exit Mass Flow Rate (kg/s)	45.17
HPC Discharge Temperature (K)	896.6
HPC Isentropic Efficiency (-)	0.812
HPC Overall Pressure Ratio (-)	23.9
High-Pressure Spool Rotational Speed (rpm)	13,265.5
Combustor Exit Temperature (K)	1715
Exhaust Gas Temperature (K)	709.2

Figure 14 shows the variation of selected HPC and engine parameters with thrust (control parameter) at SLS conditions, for four simulation options, presented in order of increasing computational complexity:

1. 0D mode using single MLC-generated map at standard temperature of $T_{std} = 288$ K.
2. 0D mode using MLC-generated maps according to actual HPC inlet temperature $T_{t,in}$
3. 1D mode with constant γ
4. 1D mode with variable gas properties

As the differences were small compared to the range of variation, the percentage difference of results from each of the first three cases from the last one is also shown.

As expected, the first option (0D map with single map) shows the largest differences (up to -0.35%) from the 1D mode with variable gas properties. The other two are well within $\pm 0.1\%$ ($\pm 0.05\%$ for the 1D mode with constant γ). The use of 0D mode with $T_{t,in}$ as an extra dimension shows the importance of obtaining the compressor performance for the actual inlet conditions and justifies the need for the 1D mode, since otherwise the 0D mode would require the generation and use of multi-dimensional tables/maps, where all possible combinations of compressor operation are included (variable geometry, bleeds, evaporation, etc.). Finally, the use of the 1D mode with constant γ proves to be an acceptable surrogate of the mode with variable gas properties, as it does not compromise the accuracy of calculations while it executes much faster. In our calculation, it was approximately 45% faster compared to the MLC with variable gas properties and in a desktop PC (Windows

10 Pro 64-bit, Intel® Core™2 Duo CPU at 3GHz with 8GB RAM) required less than 5 s for a complete engine simulation to converge to a tolerance of less than 10^{-6} . In comparison, the 0D mode executes in less than 0.05 s.

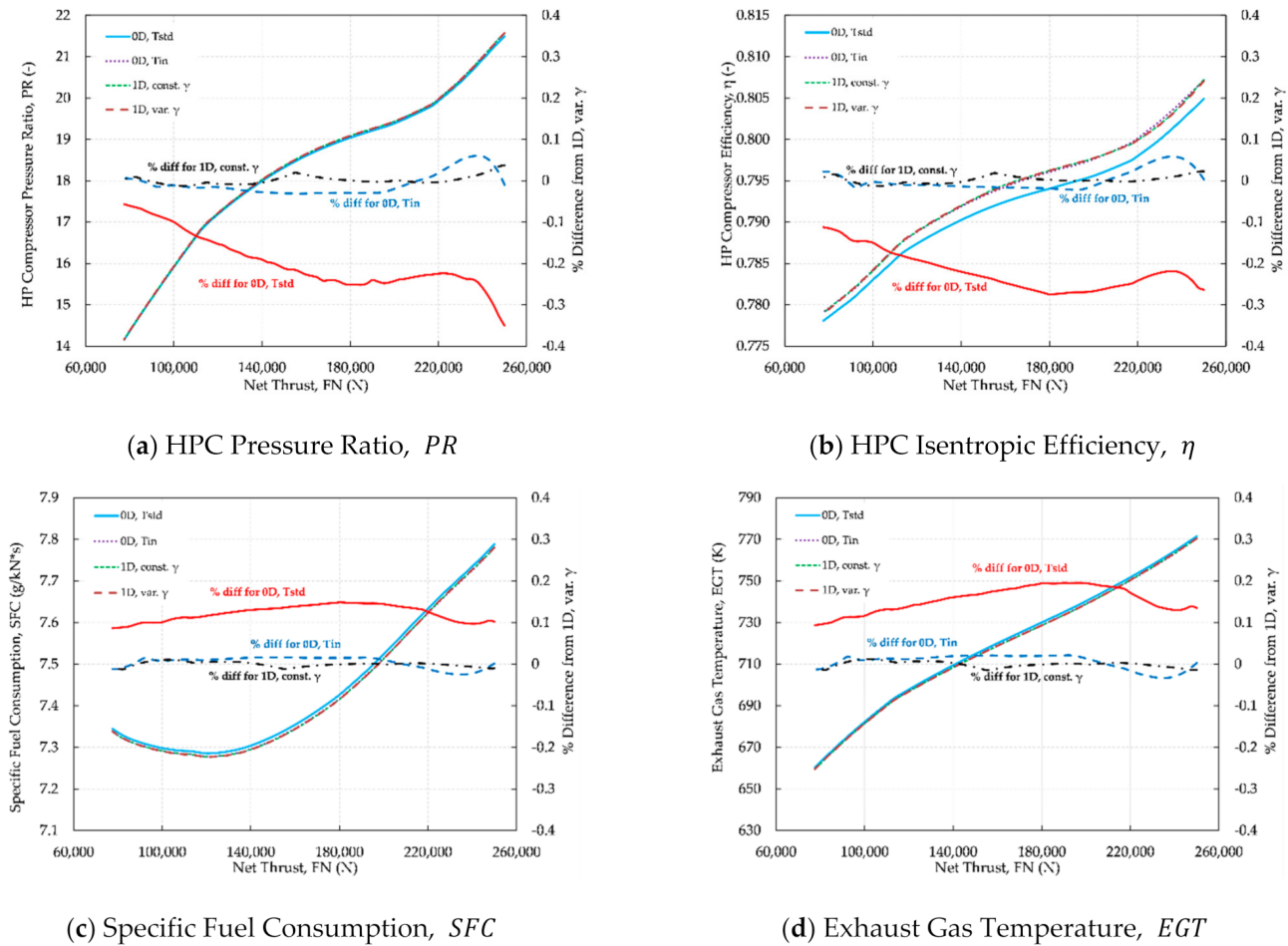


Figure 14. Comparison of results at Sea-Level Static (SLS) steady state conditions.

Repeating the same simulations at flying altitude ($ALT = 10668$ m, $M = 0.85$), similar levels of differences were observed between the different modes, as for the SLS simulations. This is demonstrated in Figure 15a for the HPC pressure ratio. However, at these conditions, there are operating points in the region of the map where the corrected speed iso-lines are almost vertical, Figure 15b. As a result, map interpolation causes a fluctuating variation of differences between 0D and 1D modes in this region. Furthermore, it is in this region that the mass flow rate correction presented in Figure 4 makes the MLC execution possible since otherwise even a small difference in mass flow rate can produce a value that is outside the working range of the 1D code.

Transient simulations at flight and SLS conditions produce similar results to the steady state ones, with differences again being slightly larger at altitude. The variation with time of the differences between the 0D (using $T_{t,in}$) and 1D (variable properties) modes for selected compressor and engine parameters is shown in Figure 16a for cruise conditions. The differences show peaks during the acceleration and deceleration parts of the simulation, which is again attributed to map interpolation, especially since in the latter case the operating line is in the region of the map where the speed iso-lines are almost vertical, Figure 16b.

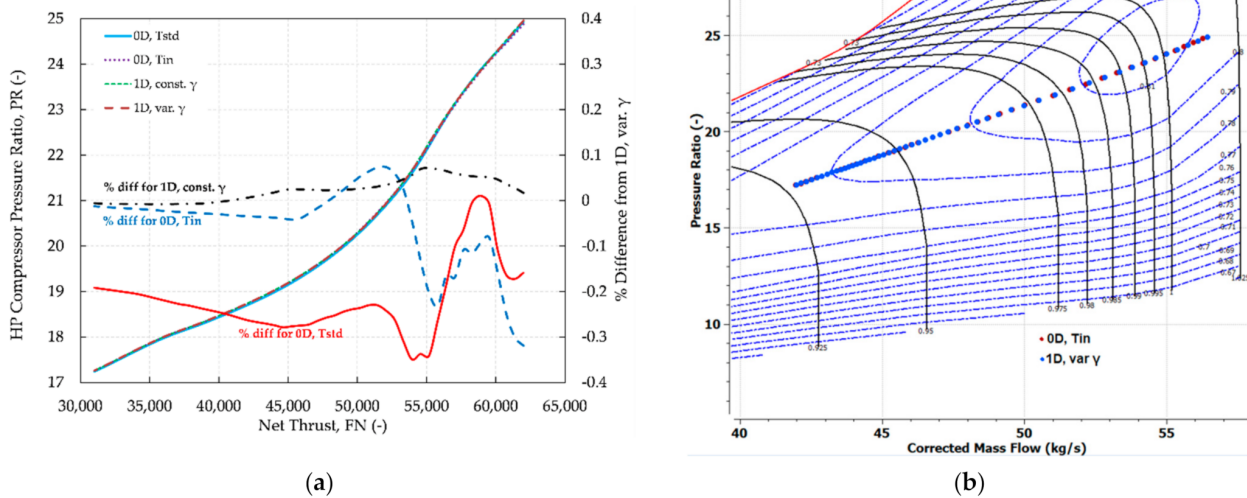


Figure 15. Results at steady state cruise conditions. (a) Variation of HPC pressure ratio with thrust; (b) 0D and 1D operating points on HPC map.

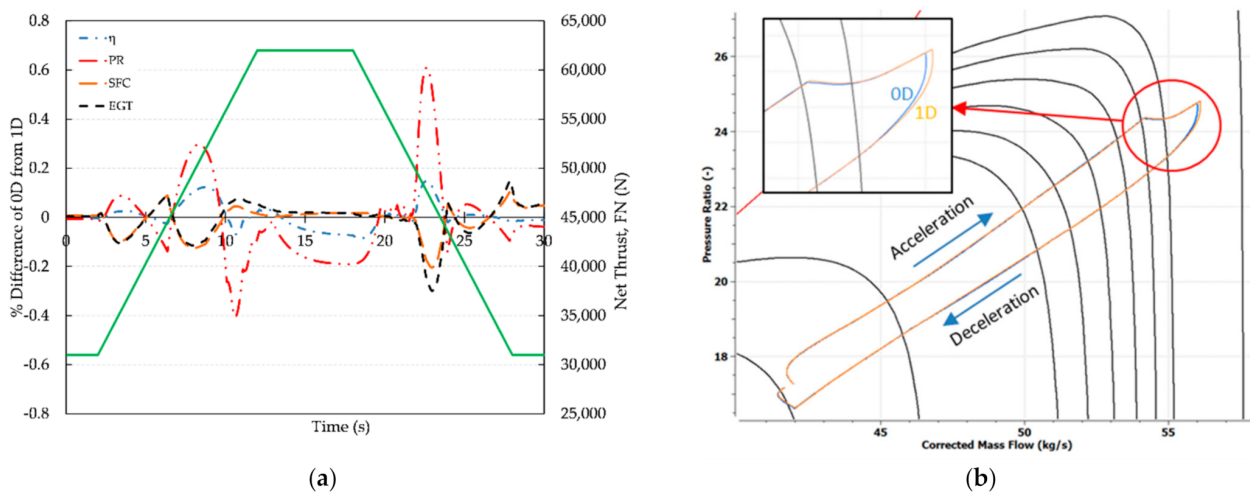


Figure 16. Results at transient cruise conditions. (a) Differences of 0D from 1D mode for selected compressor and engine parameters; (b) 0D and 1D transient operating lines on HPC map.

Finally, transition from the unchoked to the choked region and operation in the choked region was simulated at compressor component level only using the HPC 0D/1D component of the engine model. This was accomplished by simply specifying (at ISA conditions) a value for corrected speed $NcRdes$ and a range of BETA values (a total of 55 values) starting from a value in the unchoked region ($BETA = 0.6$) to a value in the choked region ($BETA = 0.05$). The component was operated in both 0D and 1D mode for two values of $NcRdes$; one which is present in the map data (95%) and one that is between existing values (96.3%). At these $NcRdes$ values, $BETA_{choke} = 0.25$. The setup of the simulation case was identical for both modes, meaning that choking was handled automatically in 1D mode as in 0D mode. Figure 17 shows the operating points on the map for each of the four cases (0D and 1D modes for the two $NcRdes$ values). For the $NcRdes$ value present in the map data (95%), the results of both 0D and 1D modes overlap on the map speed line and demonstrate that the 1D mode is capable to transition from the unchoked to the choked region and work in the choked region. This is also shown for the other $NcRdes$ value (96.3%), although map interpolation causes visible differences between the two modes, thus highlighting one of the 0D approach limitations.

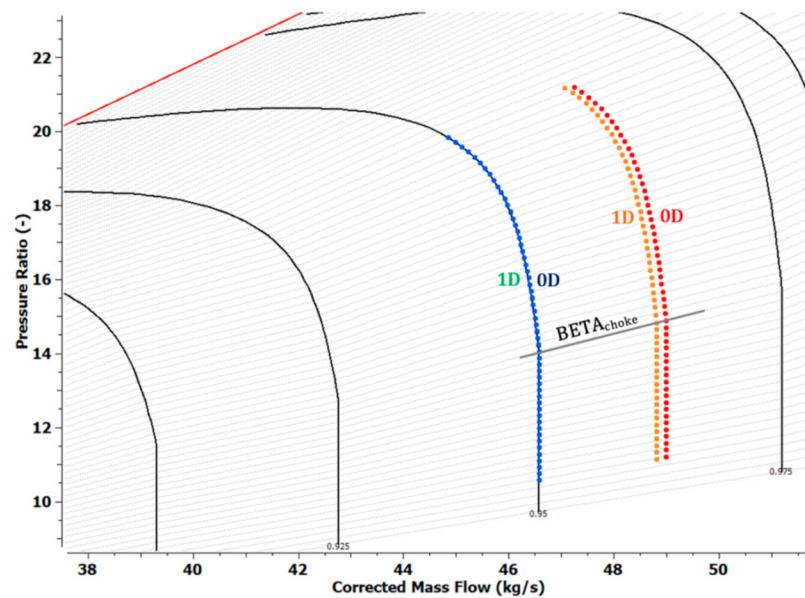


Figure 17. Operating points in map for 0D and 1D mode showing transition to choked region.

6. Conclusions

A method for modelling multistage compressor performance using a mean-line approach, covering the entire operating region that includes choked operation has been presented. The method was materialized through the development of a dedicated component in a computational environment used for gas turbine engine modelling. The approach followed allows the integration of the mean-line model at engine level, without changing the mathematical model boundary and algebraic variables of conventional 0D map architecture.

To deal with convergence problems, posed by the simplistic nature of the mean-line equations when the compressor works near or beyond choking conditions, a formulation was developed and implemented to model choking at blade row and compressor level. Furthermore, the capability was added to allow the component developed to work in both 1D and 0D modes, even within the same simulation case. The 1D component is capable of working in both the unchoked and choked regions, without any changes to the mathematical model, while the transition from one region to the other is transparent to the user. In addition, the calculation of the choke point for the current compressor operating conditions allowed a correction to be made during 1D model execution so that the influence of any secondary effects can be taken into account. The option to perform calculations at cascade level with constant γ was added using only one variable (the compressor average pressure ratio) to specify an average cascade temperature for which γ is calculated (instead of only of the inlet temperature).

Choking modelling of this level was shown, for the first time in the open literature, for the case of a multi-stage compressor for which a performance map was generated in the whole operating range. As shown, choking is calculated in a transparent way, allowing the user to know any-time where along the flow path choking has occurred and what conditions caused it.

Finally, the integration capabilities of the developed component were verified through steady state and transient simulations of a turbofan model at both altitude and SLS conditions where the new component was used as the engine's HPC in both 0D and 1D mode. Operation in the choked region and the transition from one region to the other was demonstrated at component level. In terms of simulation times, the execution of the 1D mode with constant γ and c_p halved execution time without affecting the accuracy of the results compared to the 1D mode with variable gas properties.

Author Contributions: Conceptualization, I.K., A.A., N.A., and K.M.; methodology, I.K. and A.A.; software, I.K., A.A., and N.A.; validation, I.K., A.A., and N.A.; formal analysis, I.K. and A.A.; investigation, I.K. and A.A.; resources, I.K. and A.A.; data curation, I.K., A.A., and N.A.; writing—original draft preparation, I.K. and A.A.; writing—review and editing, I.K., A.A., K.M., and N.A.; visualization, I.K. and A.A.; supervision, N.A. and K.M.; project administration, K.M. and N.A.; funding acquisition, K.M. and N.A. All authors have read and agreed to the published version of the manuscript.

Funding: This research received partial funding by SAFRAN AIRCRAFT ENGINES and own recourses.

Data Availability Statement: The data presented in this study are available on request from the corresponding author.

Acknowledgments: The authors would like to express their thanks to SAFRAN AIRCRAFT ENGINES for supporting the work that led to this paper and for allowing its publication. Thanks are expressed to J. Ruiz for many useful comments and discussions.

Conflicts of Interest: The authors declare no conflict of interest.

Nomenclature

Abbreviations

0,1,2,3D	0,1,2,3-Dimensional
AMB	Ambient
BRM	Blade Row Module
BRN	Burner
CFD	Computational Fluid Dynamics
D13/25/30/45/50	Interconnecting ducts
GE	General Electric
HP	High-Pressure
HPC	High-Pressure Compressor
HPS	High-Pressure Shaft
HPT	High-Pressure Turbine
IGV	Inlet Guide Vane
INL	Engine Inlet
ISA	International Standard Atmosphere
IVM	Inter-Volume Module
LE	Leading Edge
LP	Low-Pressure
LPC	Low-Pressure Compressor
LPS	Low-Pressure Shaft
LPT	Low-Pressure Turbine
MLC	Mean-Line Code
NASA	National Aeronautics and Space Administration
NBP	Bypass Nozzle
NCO	Core Nozzle
OTAC	Object-oriented Turbomachinery Analysis Code
PROOSIS	Propulsion Object Oriented Simulation Software
R/S	Rotor/Stator
SLS	Sea-Level Static
TE	Trailing Edge

Symbols

A	Area (m ²)
ALT	Altitude (m)
β	Flow angle relative to frame of reference (°)

γ	Specific heats ratio (–); stagger angle (°) (for loss and deviation correlations)
δ	Deviation angle (°)
δ_c	Radial clearance (m)
ε	User-defined tolerance ($\varepsilon > 0$)
η	Compressor overall isentropic efficiency (–)
η_p	Compressor overall polytropic efficiency (–)
θ	Blade camber angle (°)
ν	Prandtl-Meyer function (°)
ρ	Flow density (kg/m ³)
κ	Blade metal angle w.r.t. axial direction (°)
σ	Blade row solidity (–)
ω	Total pressure loss coefficient (–)
a	Position of blade maximum camber (m)
AVDR	Axial Velocity Density Ratio (–)
b	Blade row throat width for a single passage (m)
c_p	Heat capacity at constant pressure (J/kgK)
c	Blade chord length (m)
C_L	Blade lift coefficient (–)
BETA	Auxiliary map parameter (–)
DF_{eq}	Equivalent diffusion factor (–)
EGT	Exhaust Gas Temperature (K)
F, G	Function/ Functional
FN	Net Thrust (N)
h	Blade height (m)
i	Stage number (–); incidence angle (°)
g	Distance between two blades measured normal to chord line (m)
\dot{m}	Mass flow rate (kg/s)
M	Flow Mach number (–)
N	Compressor mechanical rotational speed (rpm)
NcRdes	Corrected speed relative to design (–)
p	Pressure (Pa)
PR	Total Pressure Ratio (–)
R	Gas constant (J/kgK)
s	Blade row pitch length (m)
SFC	Specific Fuel Consumption (g/kN·s)
t	Blade thickness (m)
T	Temperature (K)
W	Flow velocity relative to frame of reference (m/s)
Z_{stg}	Number of stages (–)
<i>Sub-/Super-scripts</i>	
1,2	Blade row inlet (1) and outlet (2)
br	Blade row
c	Corrected
des	Design conditions
ex	Compressor exit
in	Compressor inlet
inan	Blade row inlet flow annulus
LE	Blade Leading Edge
map	Map quantity
min	Minimum
std	Standard-day conditions
t	Total conditions
th	Blade row throat

<i>outan</i>	Blade row outlet flow annulus
<i>w</i>	Quantity relative to frame of reference
*	Choke conditions; design conditions (for loss and deviation correlations)

Appendix A. MLC Loss and Deviation Models

A summary of the default loss and deviation correlations used in MLC is given in Table A1.

Table A1. MLC loss and deviation correlations summary.

References	Correlation	Formula
[21]	Design incidence	$i^* = i(\theta, \sigma, \beta_1, t/c, a/c)$
[21]	Design deviation	$\delta^* = \delta(\theta, \sigma, \beta_1, t/c)$
[22]	Off-design deviation	$\delta = \delta(M_{w1}, DF_{eq})$
[26]	IGVs off-design deviation	$\delta = \delta(M_1, \theta, \sigma, \gamma, AVDR, t/c)$
[21,25]	Design profile loss corrected for Mach (s_{Ma} , a_{Ma}) and Reynolds (s_{Re} , a_{Re}) number effects	$\omega_{pr}^* = a_{Ma} + s_{Ma}s_{Re} [a_{Re} + \omega(DF_{eq})]$
[21]	Off-design profile loss	$\omega_{pr} = \omega_{pr}^* f(i - i^*)$
[24]	Shock loss	$\omega_{sh} = \omega(M_{w1}, \sigma, \beta_1, \beta_2)$
[21]	Secondary loss	$\omega_{sc} = \omega(C_L, \sigma, \beta_1, \beta_2)$
[21]	Endwall loss	$\omega_{ew} = \omega(s/h, \sigma, \beta_1, \beta_2)$
[23]	Clearance loss	$\omega_{cl} = \omega(C_L, s, h/c, \delta_c, \sigma, \beta_1, \beta_2)$
[21]	Overall loss	$\omega = \omega_{pr} + \omega_{sh} + \omega_{sc} + \omega_{ew} + \omega_{cl}$
[26]	IGVs overall loss	$\omega = \omega(M_1, \theta, \sigma, \gamma, t/c)$

Appendix B. Blade Row Throat Passage Choke Modelling

For modelling the blade row throat passage choking, two possible flow conditions at blade row inlet were examined, i.e., subsonic and supersonic. The relevant equations, used by Cumpsty and Freeman [27,28] for modelling subsonic and supersonic throat passage choking, are presented.

Choking when the inlet flow to the blade row is subsonic is determined using the simplified analysis described by Cumpsty in [27]. When the flow angle at the blade row inlet is reduced, then the mass flow through the throat passage increases and a minimum angle value can be obtained for which the blade row becomes choked. This value for β_1^* is obtained using the following equation:

$$\frac{b}{s \cos \beta_1^*} = M_{w1} \left(\frac{1 + \frac{\gamma-1}{2}}{1 + \frac{\gamma-1}{2} M_{w1}^2} \right)^{\frac{\gamma+1}{2(\gamma-1)}} \quad (A1)$$

For the supersonic inlet flow case, two possible sub-cases are identified: supersonic with detached shocks and supersonic with attached shocks. For the first case, the supersonic inlet flow leads to the formation of bow shocks that are detached from the blade row LE. For this case, the modelling proposed in [27,28] was used for obtaining β_1^* . Following a relatively simple control-volume analysis for the conservation of mass, momentum, and energy between the blade row inlet and the throat passage, and assuming that the throat is choked, Cumpsty and Freeman [27,28] arrived at the following relation, for establishing β_1^* :

$$\frac{\cos \kappa_{LE}}{\cos \beta_1^*} + \gamma M_{w1}^2 \cos(\beta_1^* - \kappa_{LE}) = M_{w1} \left(1 + \frac{\gamma-1}{2} M_{w1}^2 \right)^{\frac{1}{2}} \left(1 + \frac{\gamma-1}{2} \right)^{-\frac{1}{2}} \frac{1 + \gamma(1 - t/g)}{1 - t/g} \quad (A2)$$

which is solved iteratively to obtain β_1^* .

Finally, for supersonic inlet there is a unique flow angle for which the bow shock formed is attached at the blade row LE. For this case, an idealized flow was considered, which is described in much detail by Cumpsty in [27]. The modelling approach described

in [27] leads to the following non-linear system of equations, between the inlet flow and the end (subscript “e”) of the Prandtl–Meyer expansion fan developed due to the suction surface curvature in the region of the blade LE:

$$\beta_1^* + \nu(M_{w1}) = \kappa_{LE} + \nu(M_e) \quad (\text{A3})$$

$$F(M_{w1})\text{scos}\beta_1^* = F(M_e)(\text{scos}\kappa_{LE} - t_{LE}) \quad (\text{A4})$$

This system of equations is solved iteratively to give a unique set of β_1^* and M_e values for which the mass flow across the throat passage chokes. In Equation (A3), $\nu(M)$ is the Prandtl–Meyer function, and in Equation (A4) $F(M)$ is a flow function that expresses the corrected flow per unit area. The expression for both $\nu(M)$ and $F(M)$ can be found in [27].

It should be noted that when the blade row operates in the supersonic flow regime, the question arises, what is the type of flow that prevails with detached or attached shocks. In the present work, the type of flow was decided in terms of a Mach number value for which the two flow models gave the same value of β_1^* . This Mach number value was obtained iteratively and for supersonic Mach numbers below this value, the detached-shock model was applied, while for larger Mach number values the attached-shock one was implemented. An example of the operating regions of a throat passage obtained with this modelling approach is illustrated diagrammatically in Figure A1.

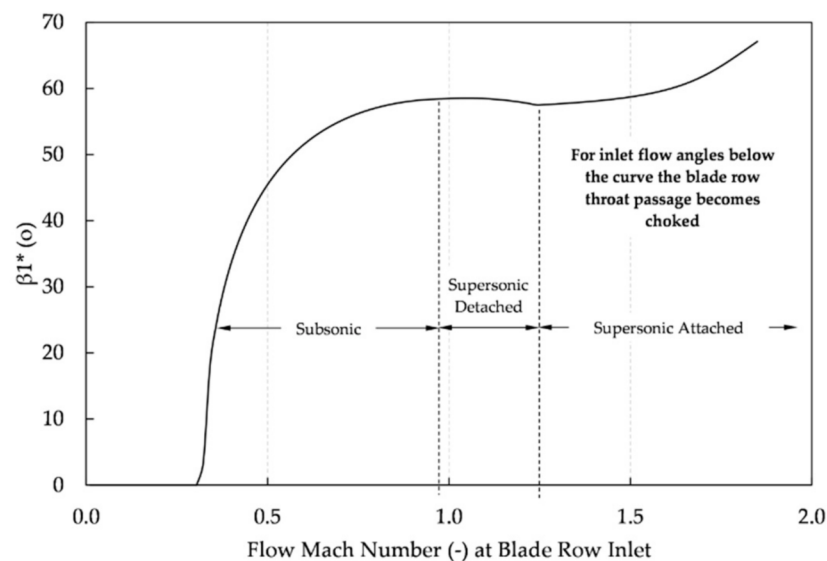


Figure A1. Example diagrammatic representation of the blade row throat choking model.

References

1. Mattingly, J.D.; Heiser, W.H.; Pratt, D.T. *Aircraft Engine Design*, 2nd ed.; AIAA: Reston, VA, USA, 2002; ISBN 1-56347-538-3.
2. Panchenko, Y.; Moustapha, H.; Mah, S.; Patel, K.; Dowhan, M.J.; Hall, D. Preliminary Multi-Disciplinary Optimization in Turbomachinery Design. In Proceedings of the RTO AVT Symposium, Paris, France, 22–25 April 2002; RTO-MP-089, 57/1-22.
3. Vieweg, M.; Wolters, F.; Reitenbach, S.; Hollmann, C.; Becker, R.-G. Multi-Disciplinary Tool Coupling for the Determination of Turbofan Transients during Preliminary Design. In Proceedings of the ASME Turbo Expo 2019, Phoenix, AZ, USA, 17–21 June 2019; GT2019-91402. [\[CrossRef\]](#)
4. Kiss, A.; Spakovszky, Z. Effects of Transient Heat Transfer on Compressor Stability. In Proceedings of the ASME Turbo Expo 2018, Oslo, Norway, 11–15 June 2018; GT2018-75413. [\[CrossRef\]](#)
5. Neumann, N.; Peitsch, D. Introduction and Validation of a Mean Line Solver for Present and Future Turbomachines. In Proceedings of the 24th ISABE Conference, Canberra, Australia, 22–27 September 2019; ISABE-2019-24441.
6. Vidal, L.E.F.; Pachidis, V.; Tunstall, R.J. Generating Axial Compressor Maps to Zero Speed. *Proc. Inst. Mech. Eng. Part A J. Power Energy* **2020**, 1–18. [\[CrossRef\]](#)

7. Zhang, Y.; Zhang, S.; Xiao, Y. Aerodynamic Performance Prediction of Transonic Axial Multistage Compressors Based on One-Dimensional Meanline Method. In Proceedings of the ASME Turbo Expo 2020, Virtual, Online, 21–25 September 2020; GT2020-14571.
8. Galvas, M.R. *FORTTRAN Program for Predicting Off-Design Performance of Centrifugal Compressors*; NASA, TN D-7487; NASA: Washington, DC, USA, 1973.
9. Jones, S.M. *Development of an Object-Oriented Turbomachinery Analysis Code within the NPSS Framework*; NASA, TM-2014-216621; NASA Glenn Research Center: Cleveland, OH, USA, 2014.
10. Jones, S.M. Design of an Object-Oriented Turbomachinery Analysis Code: Initial Results. In Proceedings of the 22nd ISABE Conference, Phoenix, AZ, USA, 25–30 October 2015; ISABE-2015-20015.
11. Veres, J.P. Axial and Centrifugal Compressor Mean Line Flow Analysis Method. In Proceedings of the 47th AIAA Aerospace Sciences Meeting, Orlando, FL, USA, 5–8 January 2009; AIAA-2009-1641. [[CrossRef](#)]
12. Hendricks, E.S. Meanline Analysis of Turbines with Choked Flow in the Object-Oriented Turbomachinery Analysis Code. In Proceedings of the 54th AIAA Aerospace Sciences Meeting, San Diego, CA, USA, 4–8 January 2016; AIAA-2016-0119. [[CrossRef](#)]
13. Arolla, S.K.; Jothiprasad, C.; Wood, T.H.; Stringfellow, A.B. Reduced Order Modeling of Choked Blade-Rows in Axial Flow Compressors. In Proceedings of the International Conference on Aerospace Science and Technology, Bangalore, India, 26–28 June 2008; INCAST 2008-002.
14. Cadrecha, D.; Chaquet, J.M.; Corral, R.; Timon, V.P. Robust Method to Solve Meanline Equations for Choked Flows. In Proceedings of the ASME Turbo Expo 2018, Oslo, Norway, 11–15 June 2018; GT2018-75362. [[CrossRef](#)]
15. Alexiou, A.; Baalbergen, E.H.; Kogenhop, O.; Mathioudakis, K.; Arendsen, P. Advanced Capabilities for Gas Turbine Engine Performance Simulations. In Proceedings of the ASME Turbo Expo 2007, Montreal, QC, Canada, 15–17 May 2007; GT2007-27086. [[CrossRef](#)]
16. Pachidis, V.; Plidis, P.; Texeira, J.; Templalexis, I. A Comparison of Component Zooming Simulation Strategies Using Streamline Curvature. *Proc. Inst. Mech. Eng. Part G J. Aerosp. Eng.* **2007**, *221*, 1–15. [[CrossRef](#)]
17. Follen, G.; auBuchon, M. *Numerical Zooming between a NPSS Engine System Simulation and a One-Dimensional High Compressor Analysis Code*; NASA, TM-2000-209913; NASA Glenn Research Center: Cleveland, OH, USA, 2000.
18. Bolemant, M.; Peitsch, D. An Alternative Compressor Modelling Method within Gas Turbine Performance Simulations. In Proceedings of the Deutscher Luft- und Raumfahrtkongress, Augsburg, Germany, 16–18 September 2014; p. 340047.
19. EcosimPro | PROOSIS Modelling and Simulation Software. Available online: <http://www.proosis.com/> (accessed on 12 December 2020).
20. Alexiou, A. *Introduction to Gas Turbine Modelling with PROOSIS*, 4th ed.; Empresarios Agrupados International (EAI) S.A.: Madrid, Spain, 2020.
21. Aungier, R.H. *Axial-Flow Compressors, A Strategy for Aerodynamic Design and Analysis*, 1st ed.; ASME: New York, NY, USA, 2003; ISBN 0-7918-0192-6.
22. Swan, W.C. A Practical Method of Predicting Transonic-Compressor Performance. *J. Eng. Power* **1961**, *83*, 322–330. [[CrossRef](#)]
23. Lakshminarayana, B. Methods of Predicting the Tip Clearance Effects in Axial Flow Turbomachinery. *J. Basic Eng.* **1970**, *92*, 467–480. [[CrossRef](#)]
24. Steinke, R.J.; Crouse, J.E. *Analytical Studies of Aspect Ratio and Curvature Variations for Axial-Flow-Compressor-Inlet Stages Under High Loading*; NASA, TN D-3959; NASA Lewis Research Center: Cleveland, OH, USA, 1967.
25. Koch, C.C.; Smith, L.H., Jr. Loss Sources and Magnitudes in Axial-Flow Compressors. *J. Eng. Power* **1976**, *98*, 411–424. [[CrossRef](#)]
26. Banjac, M.; Petrovic, M.V.; Wiedermann, A. A New Loss and Deviation Model for Axial Compressor Inlet Guide Vanes. *J. Turbomach.* **2014**, *136*, 071011. [[CrossRef](#)]
27. Cumpsty, N.A. *Compressor Aerodynamics*, 1st ed.; Longman: Harlow, UK, 1989; ISBN 0-582-01364-X.
28. Freeman, C.; Cumpsty, N.A. Method for the Prediction of Supersonic Compressor Blade Performance. *J. Propuls.* **1992**, *8*, 199–208. [[CrossRef](#)]
29. Kurzke, J.; Halliwell, I. *Propulsion and Power, An Exploration of Gas Turbine Performance Modeling*, 1st ed.; Springer: Berlin/Heidelberg, Germany, 2018; ISBN 978-3-319-75977-7.
30. Walsh, P.P.; Fletcher, P. *Gas Turbine Performance*, 2nd ed.; Blackwell Publishing: Oxford, UK, 2004; ISBN 063206434X.
31. Advisory Group for Aerospace Research & Development (AGARD). *Recommended Practices for the Assessment of the Effects of Atmospheric Water Ingestion on the Performance and Operability of Gas Turbine Engines*; AGARD-AR-332; AGARD: Neuilly-sur-Seine, France, 1995.
32. Steinke, R.J. *Design of 9.271-Pressure-Ratio Five-Stage Core Compressor and Overall Performance for First Three Stages*; NASA, TP-2597; NASA Lewis Research Center: Cleveland, OH, USA, 1986.
33. Holloway, P.R.; Knight, G.L.; Koch, C.C.; Shaffer, S.J. *Energy Efficient Engine High Pressure Compressor Detail Design Report*; NASA, CR-165558; NASA Lewis Research Center: Cleveland, OH, USA, 1982.
34. Reid, L.; Moore, R.D. *Performance of Single-Stage Axial-Flow Transonic Compressor with Rotor and Stator Aspect Ratios of 1.19 and 1.26, Respectively, and with Design Pressure Ratio of 1.82*; NASA, TP-1338; NASA Lewis Research Center: Cleveland, OH, USA, 1978.